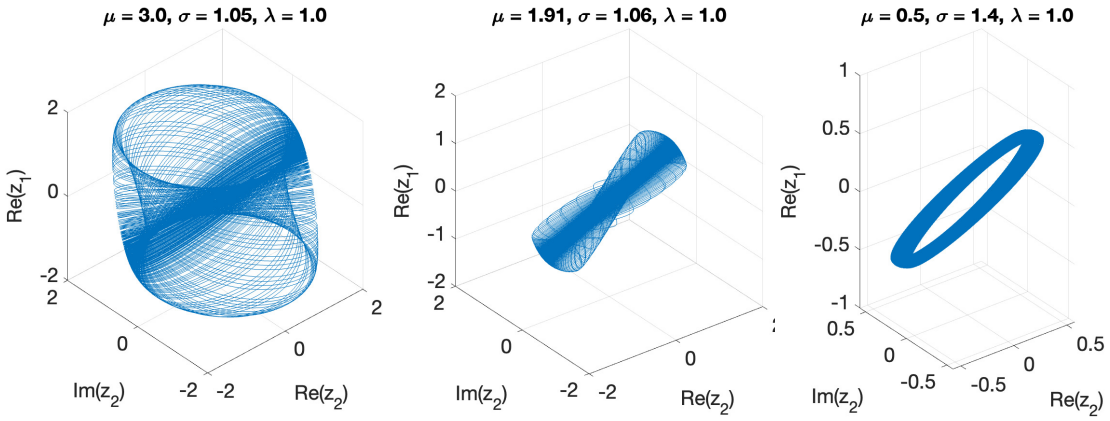

Figure 13: The invariant tori attractors of ODE (16).

- **Case $\mu + \varepsilon > 0$.** Rescaling time, introducing a new dependent variable v, and redefining the parameters as

$$\tau = \lambda\sqrt{\tfrac{\mu}{\mu+\varepsilon}}t, \quad u = v\sqrt{\mu+\varepsilon}, \quad \tilde{\mu} := \frac{\mu+\varepsilon}{\lambda}\sqrt{\frac{\mu+\varepsilon}{\mu}}, \quad \tilde{\sigma} = \frac{\sigma}{\lambda}\sqrt{\frac{\mu+\varepsilon}{\mu}}, \tag{34}$$

  we obtain the ODE for v that matches Eq. (21):

$$\dot{v} = \tilde{\mu}(1-|v|^2)v + i\tilde{\sigma}v - 1. \tag{35}$$

  Therefore, we refer the reader to Section 4.1 where a detailed analysis of this ODE is conducted.

- **Case $\mu + \varepsilon < 0$.** We redefine time, the dependent variable, and the parameters as

$$\tau = \lambda\sqrt{\tfrac{\mu}{|\mu+\varepsilon|}}t, \quad u = v\sqrt{|\mu+\varepsilon|}, \quad \tilde{\mu} := \frac{|\mu+\varepsilon|}{\lambda}\sqrt{\frac{|\mu+\varepsilon|}{\mu}}, \quad \tilde{\sigma} = \frac{\sigma}{\lambda}\sqrt{\frac{|\mu+\varepsilon|}{\mu}} \tag{36}$$

  and obtain the following ODE for v:

$$\dot{v} = -\tilde{\mu}(1+|v|^2)v + i\tilde{\sigma}v - 1. \tag{37}$$

  The ODE system for the real and imaginary components of v is

$$\begin{aligned} \dot{v}_R &= -\tilde{\mu}(1+|v|^2)v_R - \tilde{\sigma}v_I - 1, \\ \dot{v}_I &= -\tilde{\mu}(1+|v|^2)v_I + \tilde{\sigma}v_R. \end{aligned} \tag{38}$$

  Looking for equilibria of Eq. (38) and following the steps conducted in Section 4.1.2, we obtain the following equation for $|v|^2$:

$$\tilde{\mu}^2(1+|v|^2)^2|v|^2 + \tilde{\sigma}^2|v|^2 = 1. \tag{39}$$

- **Case $\mu + \varepsilon = 0$.** We redefine time, the dependent variable, and the parameters as

$$\tau = \lambda t, \quad u = v\sqrt{\mu}, \quad \tilde{\mu} := \frac{\mu}{\lambda}, \quad \tilde{\sigma} = \frac{\sigma}{\lambda} \tag{40}$$

  and obtain the ODE

$$\dot{v} = -\tilde{\mu}|v|^2 v + i\tilde{\sigma}v - 1. \tag{41}$$

The corresponding ODE system for v_R and v_I, where $v = v_R + iv_I$, is

$$\begin{aligned} \dot{v}_R &= -\tilde{\mu}|v|^2 v_R - \tilde{\sigma} v_I - 1, \\ \dot{v}_I &= -\tilde{\mu}|v|^2 v_I + \tilde{\sigma} v_R. \end{aligned} \tag{42}$$

The squared absolute value at the equilibria of Eq. (42) must satisfy

$$\tilde{\mu}^2|v|^6 + \tilde{\sigma}^2|v|^2 = 1. \tag{43}$$

Eqs. (39) and (43) have a unique solution $|v|^2 > 0$ at any positive $\tilde{\mu}^2$ and any $\tilde{\sigma}^2$, because their left-hand sides monotonously increase from zero to infinity as $|v|^2$ grows from zero to infinity, while their right-hand sides are positive constants. Eq. (39) defines a family of ellipses centered at the origin of the $(\tilde{\sigma}, \tilde{\mu})$-plane with the major semiaxis $|v|^{-1}$ in the direction of $\tilde{\sigma}$ and the minor semiaxis $(1+|v|^2)^{-1}|v|^{-1}$ in the direction of $\tilde{\sigma}$. Eq. (43) also defines a family of ellipses centered at the origin of the $(\tilde{\sigma}, \tilde{\mu})$-plane and semiaxes $|v|^{-1}$ and $|v|^{-3}$ in the directions of $\tilde{\sigma}$ and $\tilde{\mu}$, respectively. The roles of the major and minor semiaxes switch at $|v| = 1$.

The stability conditions are obtained by computing the Jacobians J of ODEs (38) and (42) and requiring that $\det J > 0$ and $\operatorname{tr} J < 0$. For ODEs (38) and (42), these conditions, respectively, are:

$$\begin{cases} \det J = & \tilde{\mu}^2(1+|v|^2)(1+3|v|^2) + \tilde{\sigma}^2 > 0 \\ \operatorname{tr} J = & -2\tilde{\mu}(1+2|v|^2) < 0 \end{cases}, \tag{44}$$

$$\begin{cases} \det J = & 3\tilde{\mu}^2|v|^4 + \tilde{\sigma}^2 > 0 \\ \operatorname{tr} J = & -4\tilde{\mu}|v|^2 < 0 \end{cases}. \tag{45}$$

These stability conditions hold for all $\tilde{\mu} > 0$, $|v|^2 > 0$, and all $\tilde{\sigma} \in \mathbb{R}$. Phase diagrams in the $(\tilde{\sigma}, \tilde{\mu})$-planes with the level sets of $|v|^2$ equilibria for the cases where $\mu + \varepsilon \neq 0$ and $\mu + \varepsilon = 0$ are shown in Fig. 15.

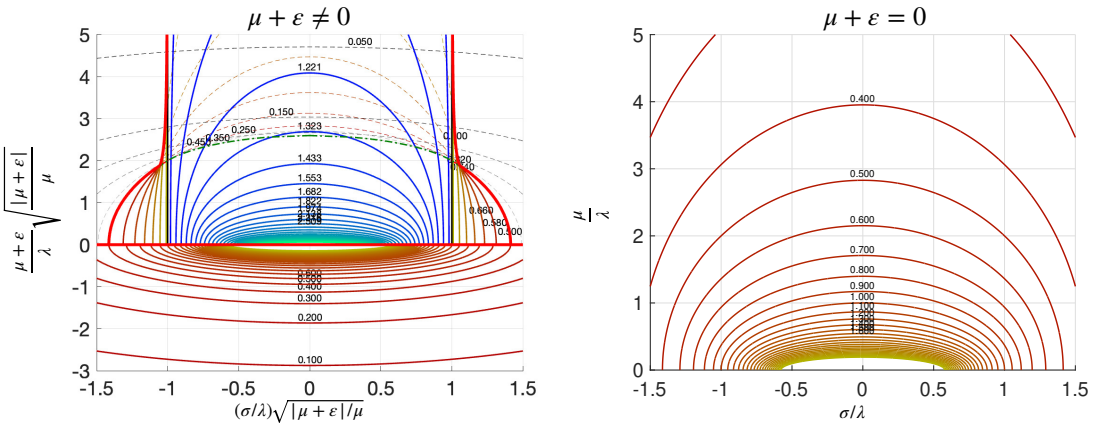

Figure 15: System (32). Phase diagrams for reduced ODEs (35) and (37), when $\mu + \varepsilon \neq 0$ (left), and (41), when $\mu + \varepsilon = 0$ (right). The solid and dashed curves are level sets of $|v|^2$ and asymptotically stable and unstable equilibria, respectively.

The dynamical properties of system (32) are summarized in the following proposition.

Proposition 2. *Consider ODE* (32) *with* $\mu > 0$ *and* $\lambda > 0$. *Suppose cell* z_1 *is at its rotating attractor* $z_1(t) = \sqrt{\mu}e^{i\omega t}$.

1. *If* $\mu + \varepsilon > 0$, *then time rescaling, variable change, and parameter redefinition in Eq.* (34) *result in ODE* (35) *in the co-rotating frame with angular velocity* ω. *ODE* (35) *coincides with ODE* (21), *and Proposition 1 holds for it.*

2. *If $\mu + \varepsilon < 0$, then time rescaling, variable change, and parameter redefinition in Eq.* (36) *result in ODE* (37) *in the co-rotating frame with angular velocity ω. At each $\tilde{\mu} > 0$ and $\tilde{\sigma} \in \mathbb{R}$, ODE* (37) *has a unique equilibrium solution. The level sets of these equilibria lie on ellipses given by Eq.* (39). *If $\tilde{\sigma} = 0$, the magnitude $|v|$ of this equilibrium blows us as $\tilde{\mu}^{-1/3}$ as $\tilde{\mu} \to 0$.*

3. *If $\mu + \varepsilon = 0$, then time rescaling, variable change, and parameter redefinition in Eq.* (40) *result in ODE* (41) *in the co-rotating frame with angular velocity ω. This ODE has a unique equilibrium solution at any $\tilde{\mu}$ and $\tilde{\sigma}$. The level sets of these equilibria lie on ellipses given by Eq.* (43). *If $\tilde{\sigma} = 0$, the magnitude $|v|$ of this equilibrium blows us as $\tilde{\mu}^{-1/3}$ as $\tilde{\mu} \to 0$.*

4.2.2 Bifurcation diagrams of the original system

The system reduction applied in Section 4.2.1 greatly simplified its analysis and reduced the hardest case with multiple periodic solutions of system (32) to the reduced system (16). However, the parameter redefinition in Eq. (34) obscures how attractors of system (32) change as we fix all parameters but one, and plot a bifurcation diagram with respect to the unfixed parameter. The simplest case is when the unfixed parameter is λ. Since both $\tilde{\sigma}$ and $\tilde{\mu}$ are inversely proportional to λ, changing λ shrinks or expands the phase diagram without changing its structure. Therefore, we will keep $\lambda = 1$ throughout this section. The second simplest unfixed parameter is σ. Since $\tilde{\mu}$ is independent of σ, and $\tilde{\sigma}$ is directly proportional to σ, the paths in the phase plane $(\tilde{\sigma}, \tilde{\mu})$ for these case are horizontal lines. Not-so-straightforward cases involve the unfixed parameters μ and ε. The corresponding paths are shown in Fig. 16, left and right, respectively. For simplicity, we will refer to these paths as μ- and ε-paths, respectively.

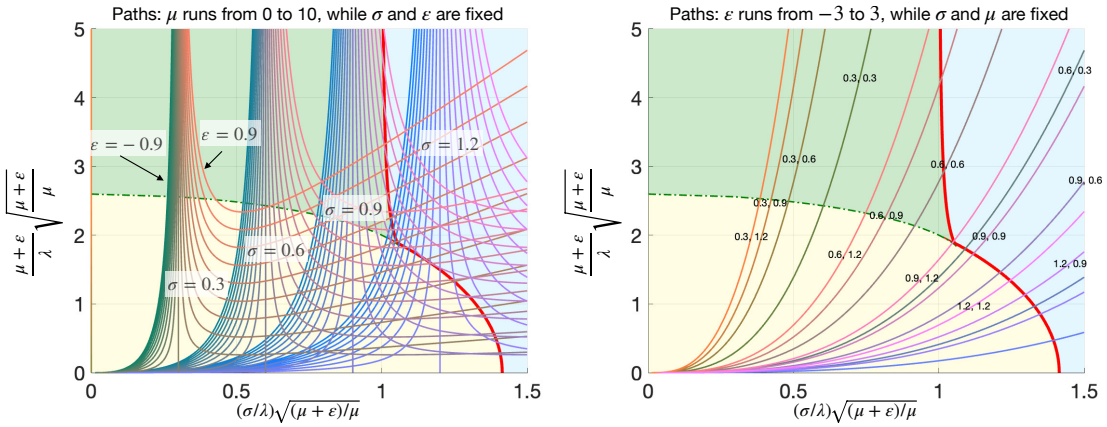

Figure 16: Left: Paths corresponding to changing μ at fixed σ and ε on the $(\tilde{\sigma}, \tilde{\mu})$-phase diagram. Paths at each fixed σ and a set of ε values $\{-0.9, -0.8, \ldots, 0.9\}$ tend to the vertical asymptote $\tilde{\sigma} = \sigma$. The paths with $\varepsilon < 0$ tend to zero as $\tilde{\mu} \to 0$, while paths with $\varepsilon > 0$ are bounded away from zero. Right: Paths corresponding to changing ε at fixed σ and μ on the $(\tilde{\sigma}, \tilde{\mu})$-phase diagram. The curves are annotated with the corresponding values of σ and μ, where the first value is σ, and the second one is μ.

The ε-paths start in the yellow region where a unique asymptotically stable periodic solution of system (32) exists and eventually enter the region with only a torus attractor. In between, they may traverse the green region with two additional unstable periodic solutions, or the tiny pink region visible in Fig. 11 with two asymptotically stable and one unstable periodic solutions of system (32).

The μ-paths may have more complex bifurcation diagrams because they may enter the region with an asymptotically stable periodic solution of system (32) multiple times. An example of such a μ-path at $\sigma = 0.98$ and $\varepsilon = 0.2$ and the resulting bifurcation diagram generated with